Experimental Noise and Vibration Analysis of Switched Reluctance Machines

Comparison of Soft and Hard Chopping in Transient Conditions

Yves MOLLET, Johan GYSELINCK

Brussels School of Engineering
Université Libre de Bruxelles (ULB)
Brussels, Belgium
ymollet@ulb.ac.be

Mathieu SARRAZIN, Herman VAN DER AUWERAER

Digital Factory – Product Lifecycle Management –
Simulation and Test Solutions
Siemens Industry Software N.V.
Leuven, Belgium

Abstract— **This paper presents a comparison of soft and hard chopping on an 8/6 SRM in terms of noise, vibration and harshness. Transient-state measurements are used to plot speed-frequency signatures of current, vibration and acoustic noise of the SRM for different load torques. With this technique speed-related frequencies can be distinguished from resonance frequencies, and therefore, more information can be extracted from the plots. The results show that hard chopping increases the loudness of acoustic noise compared to soft chopping, with a frequency shift to higher values. This however leads to an attenuation of the vibration and noise amplitudes at the most critical resonance of the SRM, situated at a relatively low frequency.**

Keywords— switched-reluctance machine; noise & vibrations; soft/hard chopping; resonance; transient condition

I. INTRODUCTION

With the development of power converters switched reluctance machines (SRMs) benefit from an increasing interest in various state-of-the-art drive configurations, such as in automotive applications [1-2].

SRMs are particular machines, with, on the one hand, concentrated windings around salient stator poles and, on the other hand, a salient rotor without any coils or magnets. Acting like an electromagnet, the excited stator winding attracts the nearest rotor poles and torque is produced until the poles are aligned (see Figure 1b). Using power electronics (generally one asymmetric H-bridge per phase, such as in Figure 5) the phases are sequentially excited in order to obtain a continuous torque. Each successive phase excitation is called 'stroke'.

Thanks to the simple stator construction (with concentrated winding) and the absence of magnets and windings in the rotor SRMs are particularly cheap [1-2, 4-8], robust [2, 4, 8, 9] and suited for severe environments [10] or high-speed applications [3]. SRMs also offer a high torque-volume ratio [4, 9] and have an inherent electrical fault-tolerance due to a negligible magnetic coupling between the phases [2, 5, 7].

However, SRMs have to cope with higher torque ripple [4-5, 7, 11] and acoustic noise and vibration [5-8, 11-12] than conventional induction or permanent-magnet synchronous machines. These drawbacks keep these motors from being extensively used so far, especially in noise-sensitive applications (such as automotive).
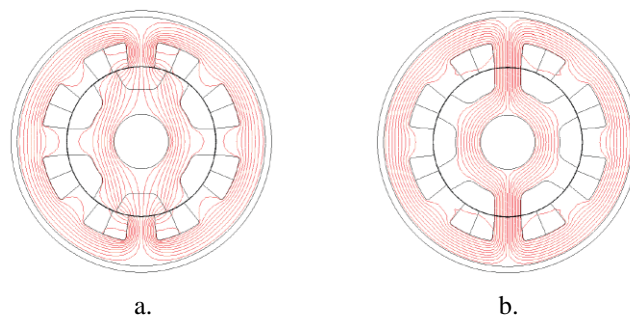

Fig. 1.   Cross-section of the investigated 8/6 SRM and flux lines for one excited phase (a. unaligned position; b. aligned position) [3]

In consequence, the future development of SRM drives will depend on the developed techniques to counter their noise, vibration and harshness (NVH) concerns. In this context, the sound quality has also to be investigated: on the one hand, tonal or narrowband and on the other hand, sharp sounds (with great high-frequency content) have especially to be avoided [6]. Possible solutions may consist of control optimization or even a new converter topology [8].

This paper proposes a comparison of soft- and hard-chopping current control techniques in terms of NVH based on current, vibration and acoustic noise measurements. Experimental tests are performed in transient conditions for different torque levels, in order to cover a wide range of the machine's working zone.

Section II presents the main characteristics and the basic control aspects of the investigated SRM as well as the origin of vibrations and acoustic noise. The proposed analysis and

measurement set-up and the experimental results are presented in section III and IV respectively.

II. Main Characteristics, Control and NVH Aspects of the Investigated SRM

A. Main characteristics of the investigated machine

The investigated machine is an 8/6 SRM. Its rated and peak power, peak torque and peak current are 15 kW, 30 kW, 200 Nm and 200 A respectively, while its maximum speed is 10 krpm. The experimental flux linkage – current curves at several rotor angles are presented in Figure 2.

B. Typical low-speed and high-speed waveforms

Referring to these flux linkage – current curves, the low-speed and high-speed waveforms of the SRM can be deduced from the voltage equation of one phase [13]:
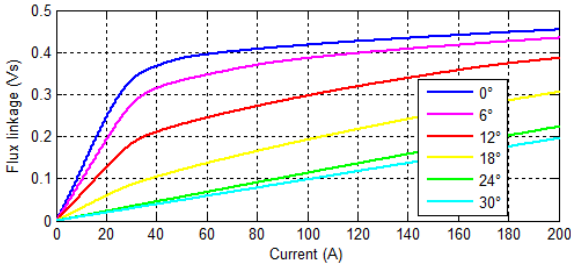
Fig. 2. Flux linkage vs. current curves for various rotor positions in mechanical degrees. The cyan and the blue curves correspond to the unaligned and to the aligned positions (cf. Figure 1a and 1b) respectively.

$$v = Ri + \frac{d\psi}{dt} = Ri + \omega\,\frac{\partial(Li)}{\partial\theta} + \frac{\partial(Li)}{\partial i}\frac{di}{dt} \quad (1)$$

in which v, i, ψ, R, L, ω, θ and t represent the phase voltage, current, flux linkage, resistance and inductance (depending on both current and rotor position as shown in Figure 2), the angular speed and position of the rotor and the time respectively. The first term of the right-hand side of (1) represents the voltage drop on the phase resistance, the second one can be considered as the back electromotive force (back-EMF) of the motor and the last one corresponds to the induced voltage due to a variation of the phase current. The produced torque is given by [13]:

$$T = \frac{\partial \int \psi di}{\partial\theta} = \frac{\partial \int Li di}{\partial\theta} \quad (2)$$

Typical waveforms corresponding to low-speed motoring mode are shown in blue in Figures 3 and 4.

At low speeds the current can be chopped at the desired value during the stroke. As the rotor is approaching the aligned position, the phase inductance increases and a positive torque (function of the applied current amplitude) is generated. In order to avoid negative torque generation, the reverse source voltage is applied before the aligned position so that the current falls back to zero.

At higher speeds the back-EMF term of (1) becomes important and the application of the full DC-bus voltage V_{dc} becomes insufficient to maintain the desired current. Only the nominal power can be maintained and the current is then controlled by adjusting the turn-on and turn-off angles at the beginning and at the end of each stroke. Typical waveforms corresponding to high-speed motoring mode are shown in red in Figure 3 and 4. There is no chopping.
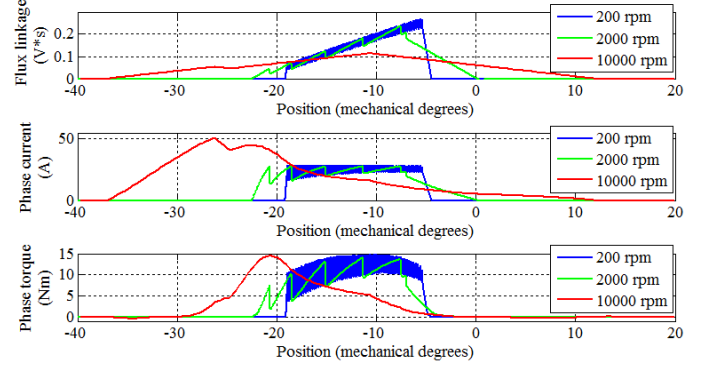
Fig. 3. Simulated flux linkage, current and torque waveforms corresponding to one phase of the investigated 8/6 SRM with 10 Nm load for different rotational speeds (in hard-chopping mode, see section C). The 0° position corresponds to the aligned position, i.e. to the geometry of Figure 1b and to the blue curve of Figure 2).
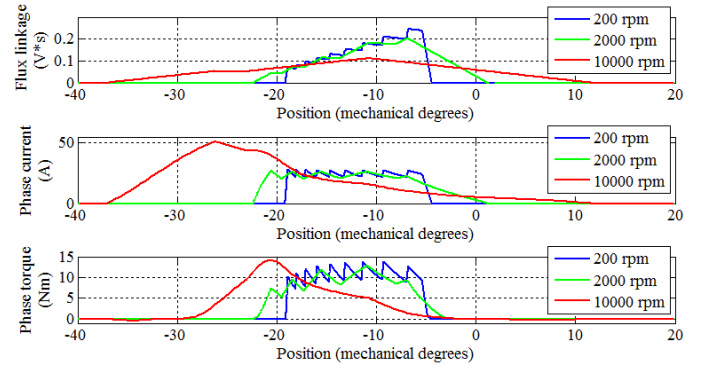
Fig. 4. Simulated flux linkage, current and torque waveforms corresponding to one phase of the investigated 8/6 SRM with 10 Nm load for different rotational speeds (in soft-chopping mode, see section C). The 0° position corresponds to the aligned position, i.e. to the geometry of Figure 1b and to the blue curve of Figure 2).

C. Hard and soft chopping

Using the classical asymmetrical H-bridge configuration, two main chopping modes are possible. In the case of hard chopping both power transistors of the asymmetric H-bridge feeding a phase are switched at the same time, applying either $+V_{dc}$ or $-V_{dc}$ to the phase (Figures 5a and 5c respectively). Examples of waveforms obtained with hard chopping are presented in Figure 3.

In soft-chopping mode one of the power transistors (T_2 in the case of Figure 5) remains on during the whole stroke, i.e.

between the turn-on and turn-off angles θ_{on} and θ_{off}, whereas the other switch (T_1 in the case of Figure 5) changes states within the stroke to chop the current. This mode results in applying either $+V_{dc}$ or a zero voltage to the phase (Figures 5a and 5b respectively). Consequently, the slope of the decaying current intervals is reduced compared to hard chopping, as shown in Figure 4. At the end of the stroke both T_1 and T_2 are switched off. $-V_{dc}$ is then applied to the phase, leading to a decrease of the phase current similar to hard chopping (cf. Figure 5c). Examples of waveforms obtained with soft chopping are presented in Figure 4.
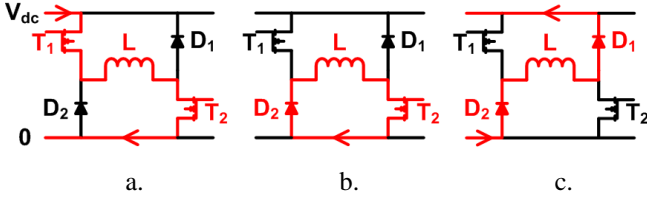

Fig. 5.   Possible conduction modes of one phase of the SRM. Depending on the states of both power switches T_1 and T_2 of the asymmetric H-bridge the applied voltage on the SRM phase winding may be $+V_{dc}$, 0 or $-V_{dc}$ (cases a, b and c respectively).

D. Control structure of the investigated SRM

At low speeds a hysteresis control is generally used to keep the current in a defined band around the reference. The DC-bus voltage V_{dc} is applied at the beginning of the stroke (turn-on angle) until the current reaches its upper limit. It is again applied when the current crosses the lower limit of the band. This control needs therefore one current sensor per phase and induces a varying switching frequency.

Due to the reduction of the current decreasing rate explained in section C, the average switching frequency is lower in soft than in hard chopping at constant hysteresis bandwidth.

Pulse-width modulation (PWM) can also be used to chop the current by imposing the PWM duty-cycle in function of the desired current [13]. This less common open-loop method is however not implemented on the bench.

The current reference value is generated and the phases are excited according to the average torque control (ATC) technique, that is, a unique current reference (corresponding to an average torque value over the stroke) is computed according to the speed and to the torque reference using a look-up table (LUT). This current set-point is dispatched between the phases according to the rotor position and to the turn-on and turn-off angles θ_{on} and θ_{off}. These angles are calculated in function of the speed and of the torque set-point value using two supplementary LUTs.

The speed control uses a classical PI controller, which outputs the reference torque. A supplementary Boolean variable is used to select soft or hard chopping. The schematic of the SRM control structure is presented in Figure 6.

E. NVH aspects

The origin of vibrations in SRMs is pulsating radial magnetic forces between stator and rotor poles, which are produced at each stroke by the sequential excitation of the phases. The use of the switching converter to control the current fed to the phases adds supplementary oscillating components at the switching frequency [6]. If the flux (and thus the current) are non-zero during commutation (e.g. at turn-off), the generated vibrations are much more important [8, 12]. The torque value also has a significant influence on both loudness and tonality and has a more limited effect on its sharpness [6].
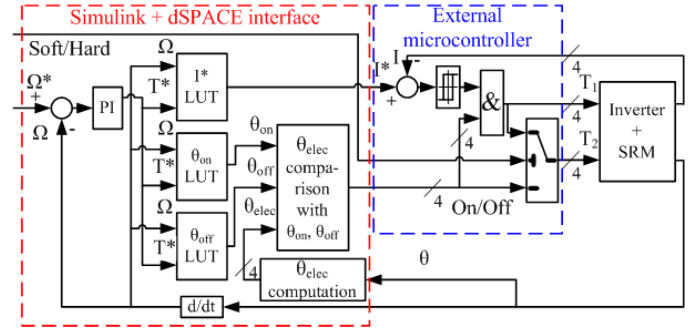

Fig. 6.   SRM test-bench control structure. The selection of the excited phase and the generation of the current reference are implemented in Simulink, while an external microcontroller performs the hysteresis control at a higher sampling rate. The T_1 and T_2 inputs of the 'Inverter + SRM' block refer to the control inputs of the upper and lower power switches in Figure 5.

Furthermore, these pulsating forces excite the natural modes of the stator [6, 8, 12] and of other components of the motor or of its environment such as, if present, the liquid cooling jacket. Certain modes can be more solicited than others depending on the number of poles in the stator [6, 9]. Sound pressure waves are also produced, generally above 1 kHz, and are responsible for the acoustic noise [6, 7]. Note that the motor mounting can also affect the natural modes by changing the stiffness of the system [6].

In order to quantify the vibrations and the associated acoustic noise, theoretical as well as simulation or experimental investigation has been performed and can be found in the literature. However, due to the complexity of the model caused by the presence of anisotropic laminated material and of cooling or mounting accessories simulation results may be unreliable, while experimental data are relatively scarce in the literature for cost reasons [7].

An experimental mapping of the natural frequencies of the stator of an 8/6 SRM is proposed in [7] comparing the classical hammer method, the use of a mini-shaker and modal analysis. In [6], the measurements on a 12/8 SRM in transient conditions enables exciting a large frequency spectrum and easily distinguishing speed orders, resonance frequencies, components linked to the switching process and background noise. Such run-ups are also used in [14] to validate an acoustic model applicable to various types of electrical machines.

III. PROPOSED ANALYSIS AND MEASUREMENT SET-UP

This paper proposes a comparison of soft and hard chopping current control techniques in terms of NVH based on current, vibration and acoustic noise measurements. Due to their ability of providing wide useful and easily distinguishable information in a limited time, experimental tests in similar transient conditions (generally in the form of run-ups) as in [6] and [14] are performed. Measurements are also taken for different torque levels, in order to cover a wide range of the machine's working zone.

The investigated SRM, controlled with a home-made converter, is coupled with a DC generator associated with its own drive and braking chopper. A commercial controllable DC supply allows for fixing a constant DC-bus voltage for the converter of the SRM. The main electric circuit of the bench is presented in Figure 7.

Both machines are controlled using an 1103 dSPACE interface. The SRM can be controlled both in soft and hard chopping thanks to an external microcontroller-based current-hysteresis control (cf. blue dashed rectangle in Figure 6). This configuration prevents the control to be affected by the low sampling frequency of the dSPACE platform (10 kHz).
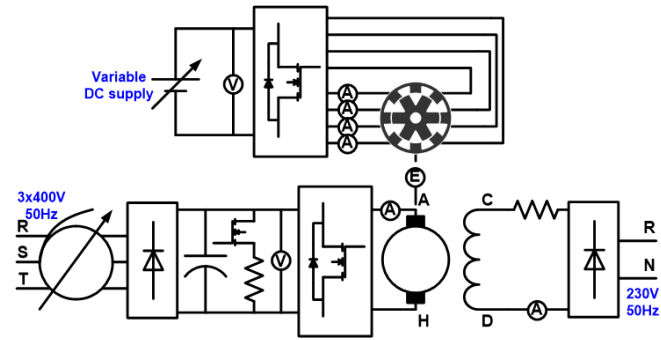

Fig. 7. Practical implementation of the test bench: main electrical circuit.

Various measurements are taken on the bench: all phase currents are measured, as well as the DC-bus voltage, while accelerometers are placed on top of both SRM and DC machines. For acoustic measurements, microphones are installed near the SRM and DC machines and near the inverter. The location on the test bench of the sensors related to the presented measurements is shown in Figure 8.
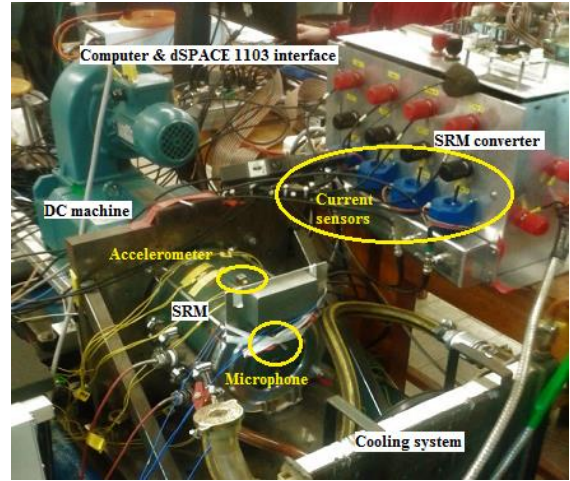

Fig. 8. Prinipal compenents of the experimental setup. The sensors considered in the presented results are circled in yellow.

IV. EXPERIMENTAL RESULTS

During the measurements, the SRM is speed controlled while the torque is imposed by the DC machine. The current hysteresis band is set to ± 2.5 A around the reference value and the DC-bus voltage of the SRM converter is 300 V.

Results are presented as waterfall diagrams to permit a global visualization of frequency content at various working points. The magnitude of the signal in dB is plotted in function of frequency (horizontal axis) and speed (vertical axis) according to a color scale.

The first results (Figures 9 to 12) show run-ups of the SRM from 200 to 2000 rpm with a rate of 25 rpm/s. The first case (Figure 9) corresponds to soft-chopping mode without load (i.e. the DC machine is not fed). As it can be seen in Figure 9, this representation easily permits distinguishing frequency content related to the speed (essentially speed orders, forming oblique green to red lines in the plot) from independent frequency content (such as external noise or resonance frequencies, appearing as vertical lines).
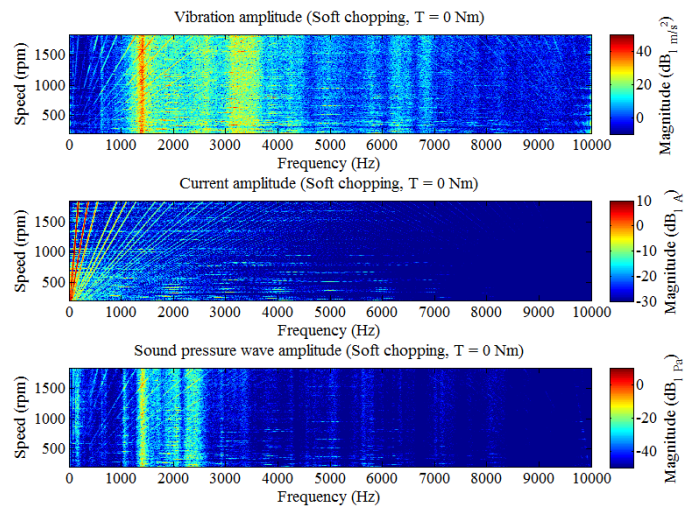
Fig. 9. Radial vibration, phase current and acoustic noise frequency content (speed-ramp test, soft chopping, no-load condition). The 0 dB references are 1 m/s^2, 1 A and 1Pa respectively.
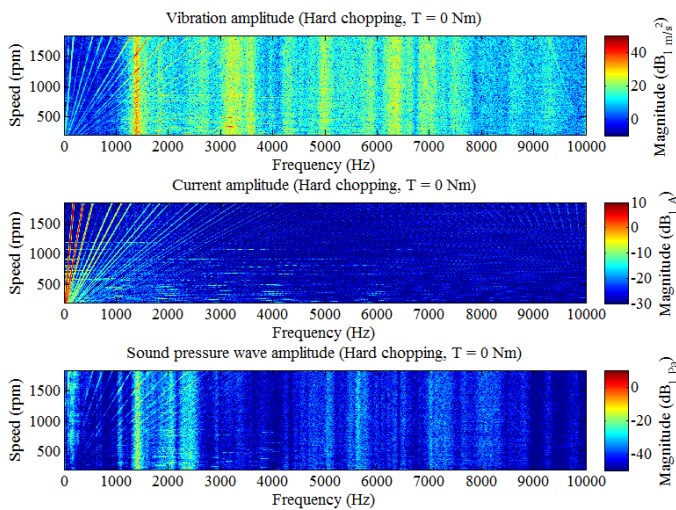
Fig. 10. Radial vibration, phase current and acoustic noise frequency content (speed-ramp test, hard chopping, no-load condition). The 0 dB references are 1 m/s^2, 1 A and 1Pa respectively.

As expected, multiples of the 6th order (corresponding to frequencies multiple of 100 Hz at 1000 rpm) are present in the current, since the current waveform is repeated each time a rotor pole is passing along the excited stator pole (i.e. six times per turn). The very limited amplitude of the 24th order and its multiples (corresponding to frequencies multiple of 400 Hz at 1000 rpm) can be explained by the fact that the current waveform is close to a square signal with a fundamental being six times the rotation frequency and with a 0.25 duty-cycle. It can easily be verified that such a square signal does not have harmonics multiple of 4.

Other oblique lines, starting at {10 kHz, 0 rpm} are also present. They are related to the presence of aliasing in the dSPACE platform.

Since the radial forces generated by the current act as a vibration source frequency, the current content can also be found in the vibration and acoustic noise plots. However, vertical bands due to resonance of the SRM or of other components of the bench also appear. The most remarkable one is the high amplitude line near 1.4 kHz, which corresponds to the ovalization mode of the machine [7, 10]. The dominance of this mode can be explained by the fact that 2 opposite poles are excited at each stroke. As expected, an amplification of the order amplitude occurs when they cross resonance frequencies. Depending on the characteristics of the mounting pieces and of the cooling jacket acoustic noise is produced with a modified spectrum (higher frequencies are generally more attenuated).

The test results presented in Figure 10 correspond to the same test conditions as in Figure 9, except that the SRM is in hard-chopping mode. The vibration and acoustic noise plots show a general increase of high-frequency content while amplitudes are slightly attenuated at frequencies lower than 3 kHz. On the current plot, some background high-frequency content also appears and the orders related to the dSPACE sampling frequency are also more visible.

The increase of high-frequency content is related to the increase of the average switching frequency in the case of hard chopping compared to soft chopping.

As it can be seen from the acoustic noise plot, the global sound amplitude is increased; however, the produced sound around the frequency of the ovalization mode is slightly reduced.

In Figures 11 and 12, results are presented for run-ups in soft- and hard-chopping modes with 10 Nm load. The application of the load generates an increase of vibration and acoustic noise amplitudes in the whole frequency range due to the increase of phase current amplitudes. Supplementary resonance frequencies are also visible, essentially between 4 and 8 kHz. The amplitudes associated with hard chopping are higher over the whole frequency range.

In the current plot, the apparition of the 24th order and its multiples (especially at high speeds) can be explained by change in current waveform compared to the low-speed case. In order to ensure the right current level is reached at the beginning of the stroke the phase has to be switched on earlier as the speed increases to compensate for the back-EMF.

Therefore, the phase current shape gets farther from ¼ duty-cycle square wave and closer to a triangular shape. This evolution with speed can be observed in the simulated currents waveforms in both hard and soft chopping (Figures 3 and 4 respectively). The importance of this phenomenon becomes greater as the torque (and the current level) increases.
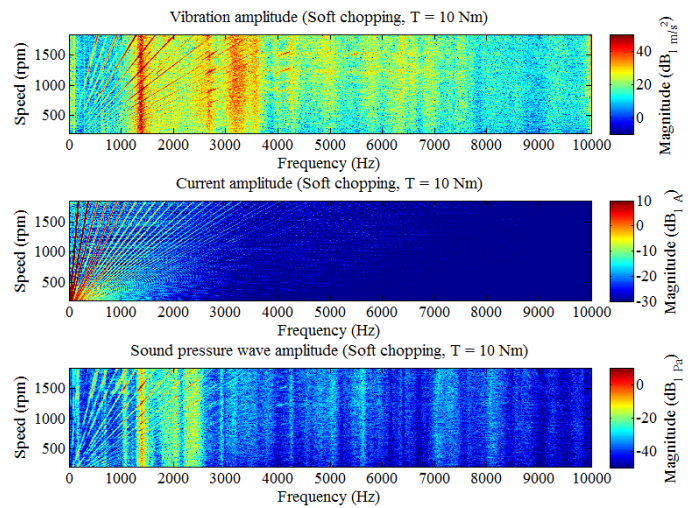

Fig. 11. Radial vibration, phase current and acoustic noise frequency content (speed-ramp test, soft chopping, with 10 Nm load). The 0 dB references are 1 m/s^2, 1 A and 1Pa respectively.
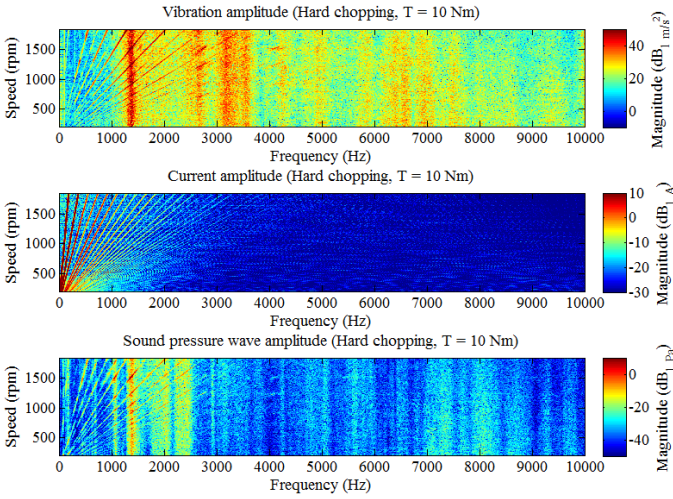
Fig. 12.   Radial vibration, phase current and acoustic noise frequency content (speed-ramp test, hard chopping, with 10 Nm load). The 0 dB references are 1 m/s^2, 1 A and 1Pa respectively.

Figures 13 and 14 present the results of torque-ramp tests at 1000 rpm in soft- and hard-chopping mode. In each case the load torque is gradually increased from 0 to 10 Nm with the DC machine with a rate of 0.5 Nm/s.

The vibration and sound pressure plots show a progressive increase of the amplitudes along the whole frequency range. Results in hard-chopping mode show globally higher amplitudes all over the torque range than in soft-chopping mode. The increase of amplitude is, however, limited up to 3500 Hz, while the dominant frequency peak remains the one of the ovalization mode near 1.4 kHz in each case.

Fig. 13.   Radial vibration, phase current and acoustic noise frequency content (torque-ramp test at 1000 rpm, soft chopping). The 0 dB references are 1 m/s^2, 1 A and 1Pa respectively.
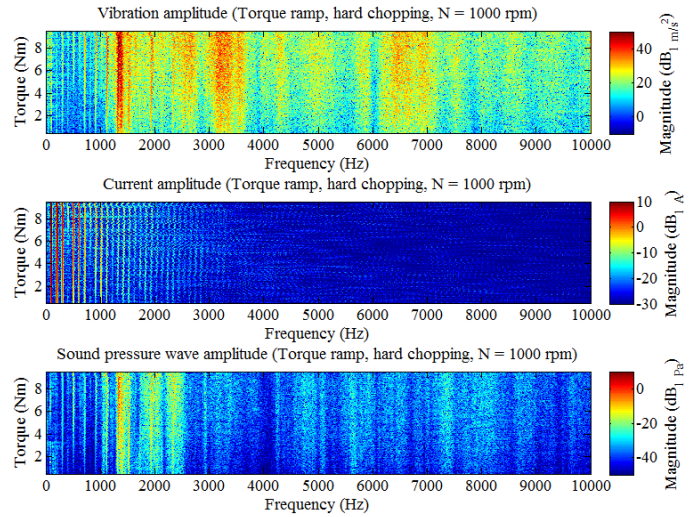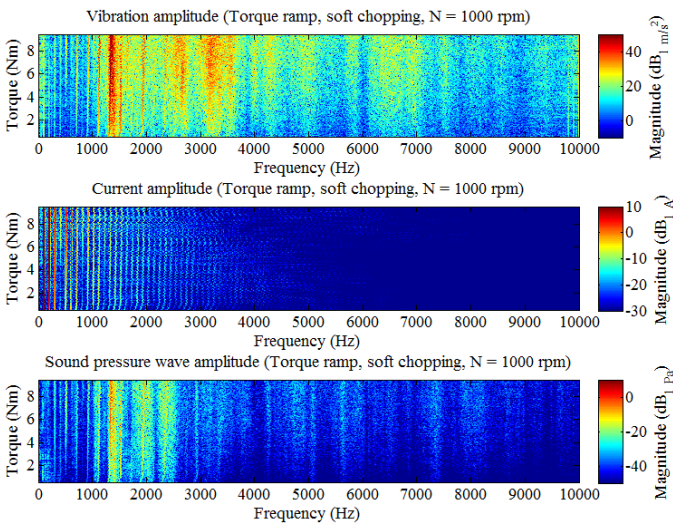

Fig. 14.   Radial vibration, phase current and acoustic noise frequency content (torque-ramp test at 1000 rpm, hard chopping). The 0 dB references are 1 m/s^2, 1 A and 1Pa respectively.

The growth of amplitudes with torque also affects the speed orders, as it can be especially seen on the current plots. For both chopping modes the 24th order and its multiples appear at a torque level around 5 Nm.

V.   CONCLUSIONS

In order to enable a global comparison of hard and soft chopping in terms of current, vibration and acoustic noise frequency content, transient-state tests (essentially run-ups, but also load-torque ramps) are performed and waterfall diagrams are used. Using this technique, frequency content linked to working conditions can be distinguished from resonance peaks.

This advanced technique is applied to compare soft and hard-chopping modes of an 8/6 SRM machine. It turns out that hard chopping globally generates higher sound pressure wave and vibration amplitudes. This increase concerns, however, especially frequencies higher than 3500 Hz. Therefore, the excitation of the most critical resonance frequency of the SRM (i.e. the ovalization mode), is not significantly affected. As expected, an increase of torque generates an increase of noise and vibration in the entire investigated frequency range.

REFERENCES

[1]   M. N. F. Nashed, "Energy efficient control technique for switched reluctance motor drives," in *Electrical Machines and Systems (ICEMS), 2012 15th International Conference on*. IEEE, 2012. p. 1–6.

[2]   X. Rain, M. Hilairet and A. Arias, 'Switched reluctance machines control with a minimized sampling frequency," Energy Conversion and Management, 2014, vol. 86, p. 701–708.

[3]   V. Petruș, "Switched reluctance motors for electric vehicle propulsion – comparative numerical and experimental study of control schemes," Ph.D. thesis, 2012.

[4]   R. H. S. Vrenken, J. L. Duarte, C. G. E. Wijnands, K. Boynov, Lomonova, S. Bervoets, and S. Faid, "Switched Reluctance Motor Drive for Full Electric Vehicles - Part I: Analysis," Ecological Vehicles and Renewable Energies (EVER), 2013 8th International Conference and Exhibition on. IEEE, 2013, p. 1–7.

[5]   G. Gallegos-Lopez, J. Walters and K. Rajashekara, "Switched reluctance machine control strategies for automotive applications", SAE Technical Paper, 2001.

[6]   M. Sarrazin, S. Gillijns, K. Janssens, H. Van Der Auweraer and K. Verhaeghe, "Vibro-acoustic measurements and techniques for electric automotive applications," in INTER-NOISE and NOISE-CON Congress and Conference Proceedings. Institute of Noise Control Engineering, 2014. p. 5128–5137.

[7]   O. P. J. Mathieu, J. Anthonis, J. Gyselinck, J. Li, Z. Song and S. Faid, "Miniature-Shaker Spectral Tests of Switched Reluctance Motor Stators," Automotive Safety and Energy Journal, 2013, vol. 4, no. 2, pp 189–197.

[8]   C. Lin and B. Fahimi, "Prediction of radial vibration in switched reluctance machines," IEEE Trans. Energy Convers, 2013, vol. 28, no 4, p. 1072–1081.

[9]   A. Hofmann, A. Al-Dajani, M. Bösing and R. W. De Doncker, "Direct instantaneous force control: A method to eliminate mode-0-borne noise in switched reluctance machines," in Electric Machines & Drives Conference (IEMDC), 2013 IEEE International. IEEE, 2013. p. 1009–1016.

[10] F. Dos Santos, J. Anthonis, F. Naclerio and J. Gyselinck, H. Van der Auweraer, L. Góes, "Multiphysics NVH Modeling: Simulation of a Switched Reluctance Motor for an Electric Vehicle,". Industrial Electronics, IEEE Transactions on, 2014, vol. 61, no 1, p. 469–476.

[11] A.-C. Pop, V. Petrus, C. S. Martis, V. Iancu and, J. Gyselinck, "Comparative study of different torque sharing functions for losses minimization in Switched Reluctance Motors used in electric vehicles propulsion", in Optimization of Electrical and Electronic Equipment (OPTIM), 2012 13th International Conference on. IEEE, 2012. p. 356–365.

[12] C. Lin and B. Fahimi, "Prediction of Acoustic Noise in Switched Reluctance Motor Drives," Energy Conversion, IEEE Transactions on, 2014, vol. 29, no 1, p. 250–258.

[13] T.J.E. Miller, "SPEED's Electrical Motors", SPEED Laboratory, University of Glasgow, 2002-2004.

[14] M. Boesing, A. Hofmann and R. W. De Doncker, "Universal acoustic modeling framework for electrical drives", 2014.